Chapter 5: Characterization of Biological and Condensed Matter at the Nanoscale

Adam R. Hall, Osama K. Zahid, Furat Sawafta, and Autumn T. Carlsen

Joint School of Nanoscience and Nanoengineering, University of North Carolina Greensboro, Greensboro, NC 27401

Abstract:

The rapid progress in nanoscience and nanoengineering over recent decades has been predicated largely on improvements in the tools used to characterize material at the nanoscale. While an abundance of new analytical techniques have been developed, a major source of future innovation will emerge from additional advances in microscopy. The microscopes used in modern nanoscience laboratories are able to image a wide range of materials (biological, non-conductive, etc.) at incredible resolution, measure and map elemental composition, elucidate fine structure, and even determine material constants. Each of these capabilities have aided researchers in both learning more about the basic nature of nanomaterials as well as using that knowledge towards a wide range of applications.

Here, we review a selection of instruments and discuss some of the unique capabilities that make them increasingly important in nanoscale research. We will concentrate on one scanning probe microscope and three different charged-particle microscopes. In each case, we will briefly describe the instrument and the mechanisms underlying its operation before detailing examples of the novel characterization techniques it has enabled.

First, we will consider Atomic Force Microscopy (AFM), a probe-based technique for imaging structures on a surface. Among the novel types of scanning probe microscopy described will be high-speed AFM, Scanning Conductance Microscopy (SCM), and Scanning Microwave Microscopy (SMM). Second, we will discuss the Transmission Electron Microscope (TEM), a microscope capable of ultra-high (atomic) resolution imaging. Here, we will detail Electron Energy Loss Spectroscopy (EELS), contrast tuning, and TEM tomography. Next, we will discuss Scanning Electron Microscopy (SEM), a widely-used instrument for material characterization. We will describe Energy Dispersive X-ray (EDX) elemental mapping as well as cathodoluminescence.

Finally, we will discuss the Helium Ion Microscope (HIM), a new technology that uses a focused beam of charged He^+ ions to image samples. We will describe its utility in high-resolution imaging, especially of biological or non-conductive samples.

5.1 Overview

There is an undeniable drive towards understanding materials and systems at nanometer length scales. Electronic devices, of course, are continually pushed toward smaller and smaller dimensions; bulk material properties are largely determined by nanoscale characteristics; and the basic functions of biology are carried out by molecular machines. For these and many other reasons, the tools of nanometrology are of increasing importance.

In this chapter, we will describe the general operation of four types of microscopy tools used in nanoscience and nanoengineering research: Atomic Force Microscopy (AFM), Transmission Electron Microscopy (TEM), Scanning Electron Microscopy (SEM), and Helium Ion Microscopy (HIM). These different instruments offer specific advantages and disadvantages in characterizing nanomaterials. Throughout the chapter, these pros and cons will be highlighted as we discuss the central components of each instrument, their general mechanisms of operation, and some selected techniques that extend their applicability in the lab.

5.2 Atomic Force Microscopy

5.2.1 Introduction and components

Atomic Force Microscopy (AFM) is one of a class of microscopes collectively referred to as scanning probe microscopes (SPMs). This family of instruments has its origin in the 1982 work of Gerd Binning and Heinrich Rohrer of IBM Zurich, who first demonstrated the Scanning Tunneling Microscope[1]. Like that earliest instrument, the majority of SPMs are able to achieve incredibly high-resolution images by operating in a manner that is very different from that of previously existing microscopes. SPMs rely on the accurate movement of a microfabricated probe across a sample surface and the collection of spatially-confined data at each location. This data can then be stitched together to form a detailed image.

AFMs, like SPMs in general, accomplish their task through the use of four main components: a sharp probe, a planar substrate, scanners, and a feedback loop (Fig. 1). Typically, the probe is fabricated using common silicon-processing techniques, resulting in a monolithic cantilever with a pyramidal or cone-shaped tip at its end. The size and shape of the cantilever can be customized for various applications and imaging modalities. The apex of the tip can be brought into intimate contact with the substrate of choice for imaging. The substrate itself must be relatively planar in order to reduce damage to both tip and sample. In order to move the tip (i) across the substrate and (ii) towards and away from the surface with a high degree of precision, piezoelectric scanners are typically used. Crystal lattice asymmetry produces a mechanical strain in piezoelectric materials when an electrical bias is applied. Scanners formed from such materials- which usually take the form of either stacks for one-dimensional actuation or cylinders for three-dimensional actuation- are able to produce tip movements with sub-nanometer accuracy. During the imaging process, the tip is scanned across the substrate surface, side to side and top to bottom, until each point is eventually probed.

The final component- the feedback loop- is a circuit that continually monitors the interaction between the probe tip and the surface and actively makes adjustments to maintain a constant level of interaction- a value known as the set point. Tip-sample interactions are recorded by reflecting a laser off the cantilever and into a quadrant photodiode. In the various modes of AFM operation (see next section), the relevant value of interaction (or setpoint) is dependent on tip-sample separation, with the feedback loop actively adjusting the position of the piezoelectric scanner perpendicular to the sample surface (*z*-direction). Plotting the amount of z-extension or retraction necessary to maintain the set point at each point (pixel) along the surface produces a topographical image.

5.2.2 Mechanisms of operation

The force experienced by a probe tip as it approaches a surface transitions from an attractive to a repulsive regime (Fig. 2) as a consequence of the transition from dominant long-range nucleus-electron interactions to dominant short-range nucleus-nucleus interactions. Using the

piezoelectric scanner, the probe tip can be positioned in either of these regimes to perform imaging in one of three possible modes: contact, intermittent contact, and non-contact.

In contact mode, the tip apex is brought into intimate static contact with the surface such that repulsion dominates. As the tip approaches the substrate, these repulsive forces act to deflect the cantilever away from its equilibrium position, and this deflection is measured as a vertical shift of the reflected laser spot across the photodiode (Fig. 3a). The position of the laser spot relative to its original (unperturbed) position acts as the set point value. If the apex encounters a feature that resides above the surface during the movement of the tip across the substrate (nominally in a plane parallel to the surface itself), repulsion will increase and thus further deflect the cantilever. The feedback loop will subsequently act to retract the cantilever position such that the set point constant is maintained (Fig. 3b-c). The inverse reaction is true for features below the surface (i.e. gutters, Fig. 3d-e). For every position of the tip, the scanner *z*-position is recorded, yielding a faithful topographic representation of the entire scanned surface.

This is the most straight-forward method used in AFM, and is thus the simplest to set up. However, several disadvantages exist. Chief among them is the potential for damage, both to the probe tip and to the substrate itself. Because the probe tip stays in close contact with the sample surface at all times, the tip can easily become worn, with the altered shape reducing resolution or possibly causing artifacts[2]. Conversely, as the tip apex is scanned and comes in contact with sample features, the strain on the sample is temporarily high until the feedback loop adjusts the cantilever position. For this reason, sample features can undergo large strains. Thus, contact mode is generally not suitable for imaging soft matter, like biological molecules.

Intermittent contact mode also utilizes the repulsive regime, but in a different manner. Here, the cantilever is driven near resonance such that the probe tip moves up and down in the *z*-direction in a continuous fashion. The amplitude of this motion can be monitored through the same laser signal described above. Geometry determines the oscillatory behavior of the cantilever and is thus an important consideration. For instance, the cantilever should be stiff enough to overcome adhesion forces during periods of contact. Otherwise, the resonant signal will be continuously perturbed. The probe tip is moved toward the substrate until the repulsive forces of close contact

damp the oscillatory motion. The level of this damping- the reduction in measured amplitude compared to the amplitude in free-space- is then used as the set point value in the feedback loop. As in contact mode, intermittent-contact imaging maps the *z*-position needed for the scanners to account for changes in repulsive force as the probe tip is scanned across the surface. Unlike in contact mode, however, the oscillatory motion of the tip confines its interaction with the substrate mainly to the vertical direction; the tip “samples” the surface at one location and then moves to the next location discretely. Since shear forces on sample features are greatly reduced, intermittent contact mode is used widely to image both hard and soft nanomaterials (Fig. 4). It should be noted, however, that some damage is still induced to both the tip and the sample, dependent on the level of damping.

Finally, non-contact mode is capable of imaging a sample using the attractive regime of atomic interaction between the probe tip and the substrate. Here, much like in intermittent-contact mode, the probe cantilever is driven near resonance (although at a comparably low amplitude). In non-contact mode, however, the cantilever is positioned at a point above the substrate such that attractive (van der Waals) forces are dominant. When the tip is scanned across the surface, these attractive forces perturb the measured amplitude signal in a separation-dependent manner, and the feedback loop again adjusts the probe *z*-position to maintain a constant value. The central advantage to non-contact mode imaging is the absence of damage to the tip or the substrate. This renders the method ideal for very delicate samples and can also result in exquisite resolution[3]. However, one disadvantage is that the tip can be perturbed by interactions with the surface or with a liquid meniscus on top of the surface. This can easily mask target features. Therefore, a pristine surface is vital in non-contact imaging and can make measurement of some biological materials challenging.

5.2.3 High-speed AFM

The High-Speed AFM (HS-AFM) technique is a novel approach to increase conventional AFM image-capture rates, allowing for visualization of unstained single biomolecule dynamics at nanometer spatial resolution and millisecond temporal resolution[4]. While a conventional AFM

requires capture rates on the order of seconds to minutes for a single frame, HS-AFM is capable of capturing more than ten frames per second[5]. The high-speed nature of this system allows for direct monitoring and recording of the behavior of various biomolecular processes, such as structural changes, and label-free molecular tracking during protein function[4,5].

In order to observe the dynamics of a system directly, various components of the conventional AFM process are replaced by smaller, more robust versions of the same components. HS-AFM incorporates small cantilevers, ~2-10 μm in length, to allow for high resonance frequency as well as lower force noise which results in smaller acquisition times per pixel[5]. Additionally, high temporal resolution is achieved by way of a high-speed piezo-scanner, which is designed to be stiff and compact via active damping and feedback controllers that allow for the maintenance of discrete tip-sample interaction forces[4]. Among the limitations that exist in the HS-AFM system is spatial resolution: large scan areas affect the quality of the resulting image due to increased tip velocity, which produces large forces that can cause damage when measuring biomolecule dynamics[5]. Other challenges include accurate enhancement of tip speed and the necessity for ultra-sharp cantilever tips.

HS-AFM has the capability to capture high-resolution videos of biomolecule activity. For instance, the structure and dynamic behavior of tail-truncated Myosin V molecules (a two-headed cargo transporter in cells) has been monitored during its motion along a protein filament[6]. The movement of the Myosin V molecules was described as “stomping-like” attachment followed by detachment of one head after another, which produced intermolecular tension and conformational switching within the motor function of the molecule throughout biomolecular processes[6]. This study was crucial to understanding both the previously expected motor movements of myosin as well as previously unknown behavior, such as the discrete movement of the uncoiling of the tail-ends of these two-headed myosin molecules.

5.2.4 Scanning Conductance Microscopy

Scanning conductance microscopy (SCM) is a technique that measures the conductance of samples at nanometer spatial resolution without the use of electrical contacts. As such, the structural and electrical properties of low- or non-conducting materials can be measured.

This dual-pass technique tracks the phase shift of a voltage-biased cantilever as a function of tip position over a sample placed above an insulating substrate and ground plane. An AFM tip passes over each line of the sample twice, first with intermittent mode AFM to obtain a topography profile, and secondly with non-contact mode at a fixed tip-surface height (typically 30-120 nm), where the topographic information from the first pass is used to maintain a constant height separation. A potential is applied between the tip and the sample during the second-pass scan, and the phase shift determined by the total capacitance at the tip provides the dielectric properties of the scanned sample as a function of height, quality factor, spring constant and tip radius[7]. The electrostatic forces that arise from the tip and substrate dictate the direction of the phase shift[8].

Applications for this technique include imaging single-wall carbon nanotubes (CNTs), distinguishing between conducting and insulating polyaniline/poly(ethylene oxide) nanofibers, and demonstrating the insulating properties of λ-DNA[7]. Characterization of these samples has shown that carbon nanotubes always show a negative phase shift while doped poly(ethylene oxide) nanofibers show an increasing positive shift with increasing fiber diameter[7]. A phase shift occurs when the tip approaches the sample and both the capacitive force and an attractive inter-atomic force act on the tip. The magnitude of these forces then determines the direction of the phase shift for a given sample size. Short carbon nanotubes, for example, experience smaller phase shifts due to decreased capacitance with respect to the ground plane than do longer nanotubes, a difference which can be explained by the division of voltage between the tip and the carbon nanotube[8]. Properties of λ-DNA were determined using carbon nanotube SCM measurements as a control on the same sample. While CNTs provide a clear signal in the sample measurements, the λ-DNA does not and is therefore verified as an electrical insulator that exhibits low conductivity[8].

5.2.5 Scanning Microwave Microscopy

Scanning Microwave Microscopy (SMM) is a measurement method that is capable of monitoring local material properties during conventional AFM imaging of a sample. SMM operates by use of a network analyzer that sends a microwave electromagnetic signal (typically 1-6 GHz) through a resonant circuit to a solid-metal or metal-coated probe tip. This tip acts as both a transmitter and receiver and can therefore measure any microwave signal that is reflected back from the sample. The electrical properties of the substrate material that is in contact with the probe tip during this measurement determines the amount of reflection that occurs. Thus, comparison of the amplitude and phase of the reflected signal to that of the generated signal can be used in conjunction with a model or calibration standard to arrive at a quantification of local dielectric constant, capacitance, impedance, and dopant density.

A measurement of this kind is performed at each point in the imaged area during the collection of topographic data using contact-mode imaging as described above. The result is simultaneous structural and electrical measurement of the surface. By way of example, Fig. 5 shows both topography and contact-capacitance spectroscopy obtained simultaneously from a calibration standard in which sample oxide thickness is decreased in a stepwise manner from top to bottom. As the thickness decreases, capacitance is found to increase due to the smaller separation between the probe and the underlying sheet layer.

5.3 Transmission Electron Microscopy

5.3.1 Introduction and components

Transmission electron microscopy (TEM) is a technique that can produce a projected image of a thin sample with a magnification up to about one million times. This instrument is among the most accurate tools for visualization at the nanoscale, reaching atomic resolution under certain conditions. In this section, we will describe the function of TEM by addressing each major component and its function in the ultimate production of an image.

At the top of the instrument column (Fig. 6), a metal source produces a coherent beam of electrons. Generally, electrons are freed from this source in one of three ways: thermionic

emission, in which increased temperature is used; field emission, in which electric field is used; or schottky emission, in which a combination of the two is used. Each type of emission has advantages and disadvantages; for instance, while a thermionic emitter has high temporal stability, the beam it produces is typically less bright and has lower phase consistency (coherence) than other emitter types. The effect of these factors must be taken into account for specific applications. After being freed from the emitter, electrons are next accelerated away from the source and down the column by a large positive voltage (typically 100-400 kV) which is applied to a solid disk electrode with an opening (the anode). The beam that emerges from the anode aperture is divergent.

Next, the beam encounters a set of electromagnetic condenser lenses. The first of these is used to converge the beam to a cross-over, creating a virtual image of the source. The second lens is used to control the angle at which the beam converges toward the sample below and thus the focal plane. These lenses (in conjunction with the following component) determine the “spot size” or the diameter of the beam that interacts with the sample. A smaller spot size will result in higher resolution, but at the expense of lowered brightness. After the condenser lenses, the beam reaches the condenser aperture. This is a small opening in a solid plate that is used to prevent high-angle electrons from passing. It is used to limit the brightness of the beam and its size can typically be determined by the user.

Following the condenser aperture, the beam interacts with the sample itself, where it is diffracted by the material as it passes through. The most severe limitation that must be taken into account with regard to the sample is its thickness; since the TEM operates via projection through a sample, obtaining an image requires that a measurable amount of the original beam passes through the sample without undergoing total internal scattering. In general, this requirement for electron transparency means that a sample must be less than about 100 nm thick to be compatible with TEM imaging. For many nanomaterials deposited from powder or liquid suspensions, this thickness is easily obtainable. However, bulk samples may also be studied by creating a thin section of the material to image. This is commonly achieved through the use of an ultramicrotome, a device composed of a sharp blade and a thermal or piezoelectric actuator. The

sample material is attached to the actuator above the cutting edge and is extended a sufficiently small distance between cuts to result in an electron transparent cross section that can be introduced to a grid or membrane for analysis. More recently, a focused beam of Ga ions has been used to sculpt thin sections of a sample that can then be transferred to a grid with micromanipulators[9,10]. This approach has the advantage of being able to target specific small areas of a sample. This section sculpting can be performed on both solid-state materials and biological materials, including whole cells (Fig. 7). With ultramicrotome, the latter are often embedded in a resin to create a bulk sample. While solid-state materials usually do not require additional treatments prior to imaging, the scattering density of many biological materials is rather low and uniform, providing insufficient contrast for direct imaging. Therefore, contrast-enhancing agents like ruthenium or osmium tetroxide are often employed to label specific components[11,12] (cf. Fig. 7).

Below the sample is the objective lens, which re-focuses the beam to a cross-over point and ultimately results in a diverging and inverted image of the transmitted beam. Importantly, the beam image at the cross-over (i.e. the back focal plane) is the diffraction pattern that results from the sample. This pattern can be used to achieve local crystallographic information about the material. The pattern can also be exploited to result in different imaging modes; by placing a small (select area) aperture at the back focal plane, the user can select either the undeflected beam (bright field) or any of the diffraction spots or areas (dark field). The latter results in an image formed predominantly from a given crystal orientation, revealing selective structural information about the sample.

After passing through the objective aperture, the beam is expanded using a set of intermediate lenses and a projector lens which collectively magnify the resulting image up to about one million times in a typical TEM. Finally, the projected beam is converted to a visible image. This is accomplished with a phosphorescent screen for normal usage and a CCD camera for digital image acquisition.

Together, the components of a TEM result in some of the highest-resolution microscopy available in the laboratory. As applied to solid-state nanomaterials, the instrument is capable of imaging

atomic rearrangement at material edges[13,14], the identification of crystalline domains in single-layer graphene[15], and even dynamic measurements of inter-shell coupling in concentrically-wrapped carbon nanotubes[16]. In the area of bionanoscience, TEM has found utility in the study of conformations of individual DNA-protein complexes[17] and has recently emerged as a tool for ultrahigh resolution imaging of samples in solution[18].

5.3.2 Electron energy loss spectroscopy

When an electron beam of known energy strikes a sample, a percentage of the incident electrons scatter inelastically. These deflected electrons lose energy through a variety of phenomena, including band transitions, plasmon excitations, and photon excitations[19]. Using an electron spectrometer, the energies of electrons transmitted through the sample can be analyzed. This process, known as electron energy loss spectroscopy (EELS), provides a wide spectrum of electron energy loss with energy resolution on the order of a few meV[20]. Careful interpretation of the spectrum reveals information like the type and number of atoms and the local atomic thickness of the sample. This method yields information averaged over the entire field of electron incidence simultaneously. In order to obtain spatial information, either analysis must be performed at discrete points across the sample, or the beam itself must be filtered to allow only select energies to contribute to the image (see following section).

5.3.3 Contrast tuning

As mentioned above, the interaction of the primary electron beam with the sample results in both electrons that have been inelastically-scattered and electrons that have transmitted without scattering. Due to the myriad different interactions that occur during inelastic scattering, the emerging electron energies can vary over a wide range (Fig. 8a), especially for thick samples. Commonly in TEM, the objective lens is not able to properly focus all energies present in the emerging beam (a distortion called chromatic aberration), resulting in a reduction in image contrast. While the objective aperture (see section 5.3.1) is able to account for this to a certain extent, the opening is generally of a fixed size and thus does not have high selectivity.

To address this lack of selectivity, a recent advance has allowed for precise energy filtering by first expanding the beam energy spatially and then using an adjustable aperture to select a given energy range. The former can be accomplished through electron optics that perform prismatic expansion of the beam. In a typical case, this requires the beam to be directed around a 90° angle, with higher energy electrons being deflected more than those with lower energy. However, it is often not ideal to divert the beam path so drastically. Therefore, an alternative approach utilizes an "omega filter"[21], so called because it diverts the beam path in the shape of the greek letter, ultimately bringing the expanded beam back to its original path (Fig. 8b). The adjustable aperture can then be placed in the beam path to allow a narrow band of energies (down to 10-20 eV wide) to pass. Importantly, this aperture can select for either unscattered electrons or any range of inelastically-scattered electrons, resulting in high contrast bright field imaging or enhancement of small or weak constituents, respectively. This approach can be utilized in the imaging of unstained biological samples, removing the effects of the staining process on structures of interest[22]. It can also be used to isolate narrow energy bands within an EELS spectrum to allow for elemental mapping (Fig. 9).

5.3.4 TEM tomography

In TEM tomography, an electron beam passes through a sample that is incrementally rotated around a central axis. The data collected is then re-assembled to form a three-dimensional image of sample composition and morphology (Fig. 10). These 3D images, or tomograms, can reveal detailed information about the organization within both crystalline and non-crystalline structures. Tomography has been used to study a wide variety of biological and inorganic specimens, ranging from viruses and cells to carbon nanotubes and nanoparticle superlattices[23]. Typically, resolution is on the scale of 5 to 30 nm, although 2.4 angstrom resolution using high-speed lasers has been reported[24].

While equilibrium structures have traditionally been the focus of tomograms, time-resolved scanning has recently been reported[25,26]. These studies have shown that morphological and mechanical motion of a structure can be reconstructed from timed snapshots collected over a

series of tilt angles.

5.4 Scanning Electron Microscopy

5.4.1 Introduction and *components*

The scanning electron microscope (SEM) has been a workhorse of nanoscale characterization for decades. While the resolution of SEM is significantly reduced compared to TEM (1-20 nm in most practical applications), the sample requirements are not as stringent with regards to thickness or vacuum environment; while TEM must operate in the high vacuum range (below 10^{-4} Pa), some SEM systems can operate near ambient conditions[27].

Many of the components of an SEM are very similar to those of a TEM: the electron source operates in the same manner (although usually at a lower accelerating voltage of 0.1-100 kV); the condenser lenses converge the beam and then form a steep-angle, narrow spot; and apertures are used to remove higher angle electrons. However, the order of these pieces is altered and there are additional components as well. Below, we will detail these differences.

A diagram of a typical SEM is shown in Fig. 11. As the beam passes through the condenser lenses, you will note that it passes through two apertures as well; the condenser aperture positioned between the lenses and the objective aperture after. Unlike in the TEM, the objective aperture is not moveable and thus does not select different areas of the beam. Both apertures are used to maximize coherency by allowing only the central (focused) region of the beam to pass.

Unlike in TEM, which uses a static electron beam to project through a sample, SEM operates by analyzing the products of beam-sample interaction at each discrete point across a sample surface. This necessitates that the beam position be actively adjustable. Therefore, following the objective aperture, the beam approaches a set of coils that can be used to deflect it. Two stacked sets of coils are needed to accomplish the task- while a single coil set can deflect (tilt) the beam, the resulting spot is elongated by the process and would result in a loss in resolution for areas away from the optical axis (Fig. 12b). Two sets working in tandem are able to tilt and shift the beam to new locations, effectively moving the virtual location of the electron source laterally (Fig. 12c). This maintains the spot shape and size.

Next the beam passes through an array of alternating (N-S) pole pieces, known as stigmators, which are arranged radially around the beam axis. These are used to control the eccentricity of the beam. When the beam spot is far from circular, resulting images can become streaked, and focus may become unachievable. This is because the size and shape of the beam determines the size and shape of pixels in the image, and eccentricity causes overlap along the major axis. In its simplest form (known as the quadrupole geometry), four elements are positioned at right angles to one another around the optical axis. Controlling the strength and asymmetry of the net field created by the stigmators can produce a circular beam cross-section. It should be noted that aberrant eccentricity can result from a number of sources, including geometrical imperfections in the shapes of the lenses, inhomogeneities in the lens material, contamination on the poles, and external magnetic fields. This variety of sources means that changes in beam eccentricity are time-variable, and therefore must be corrected for continually.

Once the beam shape is optimized, it passes through the objective lens. As in TEM, this component will form a virtual image of the source. The strength of the lens determines the focal plane of the beam and thus the size of the beam spot that interacts with the sample directly below. Minimization of the spot size results in a focused image.

As described above, the beam is rastered across the sample surface in SEM and the interaction between the primary beam and the sample material is quantified at each point by a detector, thereby determining pixel brightness. While the beam-sample interaction produces a large number of particles and photons (some of which are described in later sections), the products most commonly used for image formation in an SEM are secondary electrons and backscattered electrons. Each has a different origin and is detected in a different way.

Secondary electrons (SE) are electrons ejected from inner shells of the sample material through inelastic scattering of the primary beam. They are typically low energy (~50 eV), having received a fraction of the primary electron energy, and can only escape from depths on the order of 1-10 nm[28]. One common type of detector[29] utilizes a scintillator/photomultiplier apparatus to quantify SE production at each pixel and is positioned near the sample, but away from the optical path. At the head of this detector is a collector grid or cup that is held at a moderate positive voltage (100-

300 V) to attract produced electrons. This low voltage is selective towards SE due to their low energy, and thus does not affect the primary beam.

Backscattered electrons (BSE) are primary electrons that scatter elastically after interactions with nuclei. These tend to lose very little energy (< 1 eV) and are directed back along the optical path. Because of their high energy, BSE cannot be selectively steered toward a detector without affecting the primary beam, and so BSE detectors are typically annular detectors positioned directly around the beam path. These tend to be semiconductor materials in which electron-hole pairs are created by impinging BSE, resulting in a quantifiable current, much like in a charge-coupled device.

SEM is used widely in nanotechnology and is capable of imaging materials on the order of 1 nm (Fig. 13). However, some limitations exist. Among the most serious is sample charging[30]: for poorly conducting materials, electron charge is unable to dissipate from the sample properly and eventually floods the SE signal with a constant high count at the detector. This effect is especially prevalent with polymers and biological samples, making imaging of these materials challenging. Typically, two methods are used to compensate for sample charging. First, reducing the accelerating voltage of the primary beam can reduce the rate of charging. However, this also typically reduces the lateral resolution. Second, the sample can be coated with a thin conductive layer. This is often done by sputtering metals like AuPd, which has a small grain size of around 5 nm. However, this thin coating can mask small features on the surface.

5.4.2 Energy Dispersive X-ray imaging

Aside from SE and BSE, the primary electron beam generates various other types of radiation as it interacts with the sample. These radiative products include characteristic X-rays. Such X-rays are generated as a byproduct of SE production: when a primary electron knocks out an inner shell electron in an atom, an outer shell electron can replace it, resulting in the emission of a photon that corresponds to the energy difference between the two electron orbitals involved. There are a number of orbitals within an atom and the energy transition can occur between several of them, meaning that a single element under scrutiny releases a range of X-rays with

discrete energy. This results in a spectral “fingerprint” for a given element and allows for fast determination of the chemical composition of the sample. Since analysis is performed at each pixel, it also allows for the spatial mapping of elements within the sample through a process known as energy dispersive X-Ray (EDX) imaging[31]. An example of such analysis is shown in Fig. 14.

5.4.3 Cathodoluminescence

Cathodoluminescence (CL) occurs when the primary electron beam is focused on samples made of certain materials, resulting in emission of photons with characteristic wavelengths[32,33]. Semiconductors and insulators exhibit this phenomenon due to the presence of an intermediate gap between the conduction and the valence band, unlike conductors that do not have a gap between the conduction and the valence band. The primary beam can transfer energy to an electron in the valence band, which allows it to jump across the band gap into the conduction band. When such an electron relaxes back into the ground state conduction band, it can do so directly or it can be trapped temporarily by intrinsic traps (structural defects) or extrinsic traps (impurities) between the two bands. In either case, the relaxation results in the release of radiation with discrete energy in the form of photons. Since each element that constitutes the sample will luminesce with a unique wavelength, the sample composition as well as its impurities and defects can be determined with the spatial resolution of SEM.

CL has been used to characterize nanostructures such as nanorods and nanowires. For example, ZnO nanostructures formed under various conditions have been investigated[34]. Structural variations in the nanomaterials were identified by analysis of CL spectra and intensity.

5.5 Helium ion microscopy

5.5.1 Introduction and components

The helium ion microscope (HIM) is a relatively new instrument for the characterization of nanomaterials[35]. The optics (Fig. 15) and mechanism of image formation are similar to those found in SEM with one central difference: rather than an electron beam, the HIM uses a coherent

beam of He^+ ions. By the de Broglie relation, the wavelength of He^+ ions is much smaller than that of electrons, and would therefore be expected to yield an increased resolution according to the Rayleigh criterion. While a higher resolution is indeed achieved (down to 0.3 nm edge resolution), it is more a result of practical advantages, as discussed below. Regardless, HIM is capable of imaging a variety of materials with nanoscale features (Fig. 16).

The beam originates at a field ion source[36] that is generated to come to an atomically small point (Fig. 15, inset). A voltage applied to the metal tip first polarizes and then ionizes trace amounts of He gas injected around it. The enhanced field gradient at the sharpest point results in the highest ionization, and thus a large ion current is produced from the atoms at the apex. A select area aperture allows the beam produced at a single source atom to proceed through subsequent optics. Due to the large mass of He relative to electrons, the electromagnetic lenses used in SEM must be replaced with stronger electrostatic lenses in HIM. However, the interaction of the ion beam with the sample yields SE and backscattered ions that can be detected through means similar to those described previously.

An important aspect of the interaction is that He^+ ions scatter significantly less as they penetrate the sample material. This offers two specific advantages over SEM. Because the primary electrons in SEM scatter significantly, they generate SE emission from a lateral area of the sample surface that is large compared to the spot size of the beam. The low scattering of He^+ ions means that SE are produced only from an area that is roughly the size of the focal spot. This is central explanation for the incredible resolution of HIM. Second, because the He^+ beam penetrates deep into the sample, the build-up of charge at the surface is slow, even for poorly conducting samples. For this reason, imaging of polymers and biological material can be performed even without a conductive layer (cf. Fig. 16), thereby avoiding the possibility of surface structure modifications caused by metallization. An additional electron beam can also be used to counter the accumulation of positive charge, further reducing the effect.

5.5.2 Applications to nanofabrication

The momentum of He^{+} ions impinging on the sample can cause significant structural damage. While this is certainly a disadvantage for the imaging of small and delicate features (especially at high magnification and thus high ion density), the effect can also be exploited as a means to modify materials at the nanometer scale controllably. An early demonstration of this ability showed that graphene sheets could be patterned with high precision[37], including the fabrication of electrical devices[38]. HIM modification has also been applied to thin, free-standing silicon nitride membranes. At relatively low ion exposure, a membrane can be controllably thinned to a desired dimension[39]. At higher point exposure, through-holes can be fabricated with diameters below 4 nm[40]. These nanopores can subsequently be used as devices with which to characterize biological molecules electrically one at a time.

5.6 Conclusions

In this chapter, we have provided a brief introduction to a range of characterization tools used in both biological and condensed matter nanotechnology. The atomic force microscope is an instrument in which a sharp tip is scanned across a surface and probes its topography with nanometer accuracy. We discussed the various modes of AFM operation as well as two variations- high-speed AFM and scanning conductance microscopy- that add to the utility of the technique. The transmission electron microscope uses a coherent beam of electrons passed through a thin sample to form a projected image. It is compatible with both solid-state and biological materials to varying extents and offers extraordinary resolution, reaching the atomic scale. We further described electron energy loss spectroscopy, contrast tuning, and tomography as additional capabilities. The scanning electron microscope rasters an electron beam across a sample and quantifies the interaction of the primary beam with the surface material at every discrete point to form an image of the entire sample. Normal imaging is accomplished by detecting secondary electrons or backscattered electrons, but other types of radiation produced through the interaction can also be used. For instance, we describe the analysis of resultant photons both in the X-ray range (energy dispersive X-ray imaging) and in other ranges (cathodoluminescence). Finally, we described the new technology of helium ion microscopy, in

which a coherent beam of He^+ ions is used to perform scanning charged particle microscopy in the same fashion as SEM. This instrument achieves high-resolution imaging and can be used for nanoscale fabrication as well.

References

1. Binning, G., Rohrer, H., Gerber, C. & Weibel, E. Surface Studies By Scanning Tunneling Microscopy. *Physical Review Letters* **49**, 57-61, 1982.
2. Grutter, P., Zimmermannedling, W. & Brodbeck, D. Tip Artifacts Of Microfabricated Force Sensors For Atomic Force Microscopy. *Applied Physics Letters* **60**, 2741-2743, 1992.
3. Gross, L., Mohn, F., Moll, N., Schuler, B., Criado, A., Guitian, E., Pena, D., Gourdon, A. & Meyer, G. Bond-Order Discrimination by Atomic Force Microscopy. *Science* **337**, 1326-1329, 2012.
4. Ando, T., Uchihashi, T., Kodera, N., Yamamoto, D., Miyagi, A., Taniguchi, M. & Yamashita, H. High-speed AFM and nano-visualization of biomolecular processes. *Pflugers Archiv-European Journal of Physiology* **456**, 211-225, 2008.
5. Katan, A.J. & Dekker, C. High-Speed AFM Reveals the Dynamics of Single Biomolecules at the Nanometer Scale. *Cell* **147**, 979-982, 2011.
6. Kodera, N., Yamamoto, D., Ishikawa, R. & Ando, T. Video imaging of walking myosin V by high-speed atomic force microscopy. *Nature* **468**, 72-76, 2010.
7. Staii, C., Johnson, A.T. & Pinto, N.J. Quantitative analysis of scanning conductance microscopy. *Nano Letters* **4**, 859-862, 2004.
8. Bockrath, M., Markovic, N., Shepard, A., Tinkham, M., Gurevich, L., Kouwenhoven, L.P., Wu, M.S.W. & Sohn, L.L. Scanned conductance microscopy of carbon nanotubes and lambda-DNA. *Nano Letters* **2**, 187-190, 2002.
9. Giannuzzi, L.A., Drown, J.L., Brown, S.R., Irwin, R.B. & Stevie, F. Applications of the FIB lift-out technique for TEM specimen preparation. *Microscopy Research and Technique* **41**, 285-290, 1998.

10. Giannuzzi, L.A. & Stevie, F.A. A review of focused ion beam milling techniques for TEM specimen preparation. *Micron* **30**, 197-204, 1999.

11. Angermuller, S. & Fahimi, H.D. Imidazole-Buffered Osmium-Tetroxide - An Excellent Stain For Visualization Of Lipids In Transmission Electron-Microscopy. *Histochemical Journal* **14**, 823-835, 1982.

12. van den Bergh, B.A.I., Swartzendruber, D.C., Bosvander Geest, A., Hoogstraate, J.J., Schrijvers, A., Bodde, H.E., Junginger, H.E. & Bouwstra, J.A. Development of an optimal protocol for the ultrastructural examination of skin by transmission electron microscopy. *Journal of Microscopy-Oxford* **187**, 125-133, 1997.

13. Fischbein, M.D. & Drndic, M. Electron beam nanosculpting of suspended graphene sheets. *Applied Physics Letters* **93**, 113107, 2008.

14. Song, B., Schneider, G.F., Xu, Q., Pandraud, G., Dekker, C. & Zandbergen, H. Atomic-Scale Electron-Beam Sculpting of Near-Defect-Free Graphene Nanostructures. *Nano Letters* **11**, 2247-2250, 2011.

15. Huang, P.Y., Ruiz-Vargas, C.S., van der Zande, A.M., Whitney, W.S., Levendorf, M.P., Kevek, J.W., Garg, S., Alden, J.S., Hustedt, C.J., Zhu, Y., Park, J., McEuen, P.L. & Muller, D.A. Grains and grain boundaries in single-layer graphene atomic patchwork quilts. *Nature* **469**, 389-392, 2011.

16. Lin, L.T., Cui, T.R., Qin, L.C. & Washburn, S. Direct Measurement of the Friction between and Shear Moduli of Shells of Carbon Nanotubes. *Physical Review Letters* **107**, 206101, 2011.

17. Mastrangelo, I.A., Courey, A.J., Wall, J.S., Jackson, S.P. & Hough, P.V.C. Dna Looping And Sp1 Multimer Links - A Mechanism For Transcriptional Synergism And Enhancement. *Proceedings of the National Academy of Sciences of the United States of America* **88**, 5670-5674, 1991.

18. de Jonge, N. & Ross, F.M. Electron microscopy of specimens in liquid. *Nature Nanotechnology* **6**, 695-704, 2011.

19. Scholl, J.A., Koh, A.L. & Dionne, J.A. Quantum plasmon resonances of individual metallic nanoparticles. *Nature* **483**, 421-427, 2012.

20. Egerton, R.F. Electron energy-loss spectroscopy in the TEM. *Reports on Progress in Physics* **72**, 016502, 2009.

21. Probst, W., Benner, G., Bihr, J. & Weimer, E. An Omega Energy Filtering TEM - Principles And Applications. *Advanced Materials* **5**, 297-300, 1993.

22. Debruijn, W.C., Sorber, C.W.J., Gelsema, E.S., Beckers, A.L.D. & Jongkind, J.F. Energy-Filtering Transmission Electron-Microscopy Of Biological Specimens. *Scanning Microscopy* **7**, 693-709, 1993.

23. Midgley, P.A. & Dunin-Borkowski, R.E. Electron tomography and holography in materials science. *Nature Materials* **8**, 271-280, 2009.

24. Scott, M.C., Chen, C.C., Mecklenburg, M., Zhu, C., Xu, R., Ercius, P., Dahmen, U., Regan, B.C. & Miao, J.W. Electron tomography at 2.4-angstrom resolution. *Nature* **483**, 444-447, 2012.

25. Kwon, O.H. & Zewail, A.H. 4D Electron Tomography. *Science* **328**, 1668-1673, 2010.

26. Su, D.S. Electron Tomography: From 3D Statics to 4D Dynamics. *Angewandte Chemie-International Edition* **49**, 9569-9571, 2010.

27. Stokes, D.J. Recent advances in electron imaging, image interpretation and applications: environmental scanning electron microscopy. *Philosophical Transactions of the Royal Society of London Series a-Mathematical Physical and Engineering Sciences* **361**, 2771-2787, 2003.

28. Seiler, H. Secondary-Electron Emission In The Scanning Electron-Microscope. *Journal of Applied Physics* **54**, R1-R18, 1983.

29. Everhart, T.E. & Thornley, R.F.M. Wide-band detector for micro-microampere low-energy electron currents. *Journal of Scientific Instruments* **37**, 246-248, 1960.

30. Fitting, H.-J., Touzin, M., Cornet, N., Goeuriot, D., Juvé, D. & Guerret-Piécourt, C. Non-conductive sample charging in SEM and ESEM. *Microscopy and Microanalysis* **13**, 76-77, 2007.

31. Anderhalt, R. "X-ray Microanalysis in Nanomaterials". in *Scanning Microscopy for Nanotechnology: Techniques and Applications* (eds. Zhou, W. & Wang, Z.), Springer, 2006.

32. Bresse, J.F., Remond, G. & Akamatsu, B. Cathodoluminescence microscopy and spectroscopy of semiconductors and wide bandgap insulating materials. *Mikrochimica Acta* **13**, 135-166, 1996.

33. Remond, G., Cesbron, F., Chapoulie, R., Ohnenstetter, D., Roquescarmes, C. & Schvoerer, M. Cathodoluminescence Applied To The Microcharacterization Of Mineral Materials - A Present Status In Experimentation And Interpretation. *Scanning Microscopy* **6**, 23-68, 1992.

34. Grym, J., Fernandez, P. & Piqueras, J. Growth and spatially resolved luminescence of low dimensional structures in sintered ZnO. *Nanotechnology* **16**, 931-935, 2005.

35. Scipioni, L., Stern, L.A., Notte, J., Sijbrandij, S. & Griffin, B. Helium ion microscope. *Advanced Materials & Processes* **166**, 27-30, 2008.

36. Scipioni, L., Alkemade, P., Sidorkin, V., Chen, P., Maas, D. & van Veldhoven, E. The Helium Ion Microscope: Advances in Technology and Applications. *American Laboratory* **41**, 26-28, 2009.

37. Bell, D.C., Lemme, M.C., Stern, L.A., Rwilliams, J. & Marcus, C.M. Precision cutting and patterning of graphene with helium ions. *Nanotechnology* **20**, 455301, 2009.

38. Lemme, M.C., Bell, D.C., Williams, J.R., Stern, L.A., Baugher, B.W.H., Jarillo-Herrero, P. & Marcus, C.M. Etching of Graphene Devices with a Helium Ion Beam. *Acs Nano* **3**, 2674-2676, 2009.

39. Marshall, M.M., Yang, J. & Hall, A.R. Direct and Transmission Milling of Suspended Silicon Nitride Membranes With a Focused Helium Ion Beam. *Scanning* **34**, 101-106, 2012.

40. Yang, J., Ferranti, D.C., Stern, L.A., Sanford, C.A., Huang, J., Ren, Z., Qin, L.-C. & Hall, A.R. Rapid and precise scanning helium ion microscope milling of solid-state nanopores for biomolecule detection. *Nanotechnology* **22,** 285310, 2011.

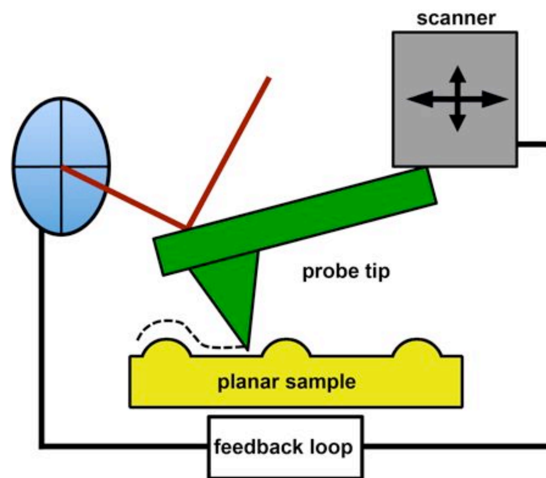

Figure 1. Schematic illustration of atomic force microscopy A sharp probe tip (green) is scanned across a planar sample surface (yellow). At each point, the probe-sample interaction is determined and kept at a constant value ("set point") by feedback control of the vertical position of the tip by the scanner (gray).

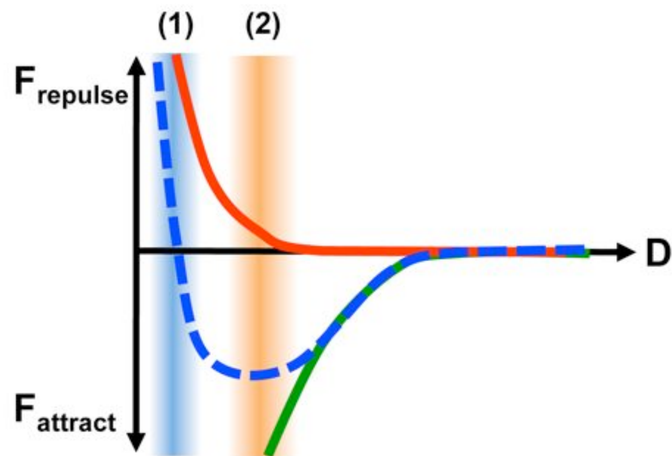

Figure 2. Tip-sample force regimes Plot describing the interplay of attractive and repulsive inter-atomic forces acting on the probe tip as a function of tip-sample distance, *D*. The green line represents electron-nucleus attraction and the red line represents nucleus-nucleus repulsion. At small separations (1), forces are net repulsive, while at slightly larger separations (2), they transition to net attractive.

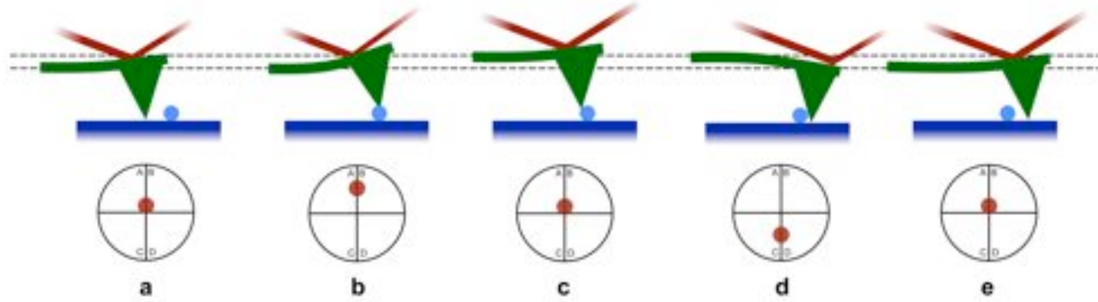

Figure 3. Set point maintenance A diagram of feedback control of laser position on a quadrant photodiode in contact mode imaging. Below each state is a snapshot of laser position on the photodiode. (a) The tip is in contact with the sample surface, resulting in an initial laser position. (b) As the tip moves over a feature, the cantilever must deflect, resulting in a shift in laser position. (c) In order to compensate, the scanner retracts the tip slightly (to the upper dashed line), returning the laser to its initial position. (d) As the tip moves off of the feature (or into a depression on the sample surface), the cantilever deflects downward, resulting in laser position movement. (e) The scanner compensates by moving the tip down (to the lower dashed line), again returning the laser spot to its initial position. Figure based on contact mode imaging.

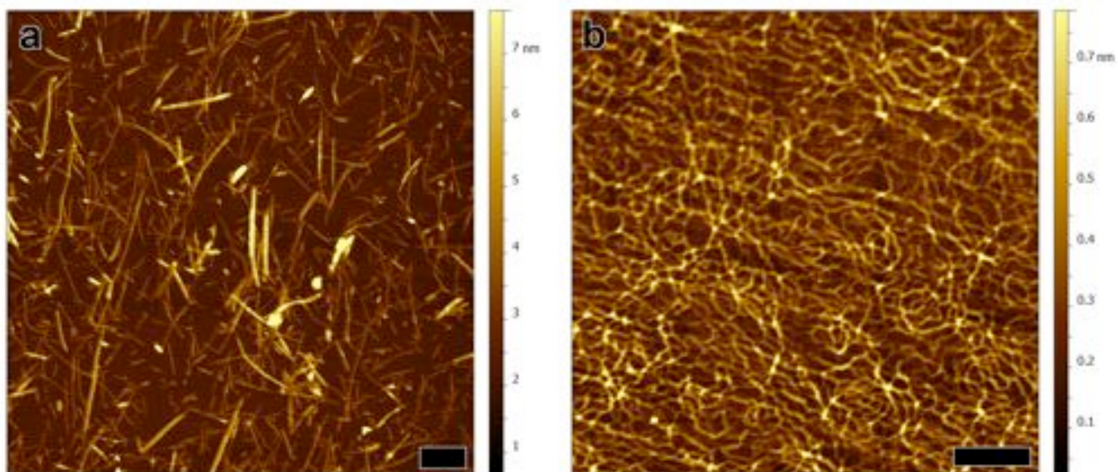

Figure 4. Intermittent contact images (a) Polydisperse carbon nanotubes (scale bar is 1 μm). (b) A dense layer of double-strand DNA (scale bar is 500 nm). Both materials are deposited on a cleaved mica surface.

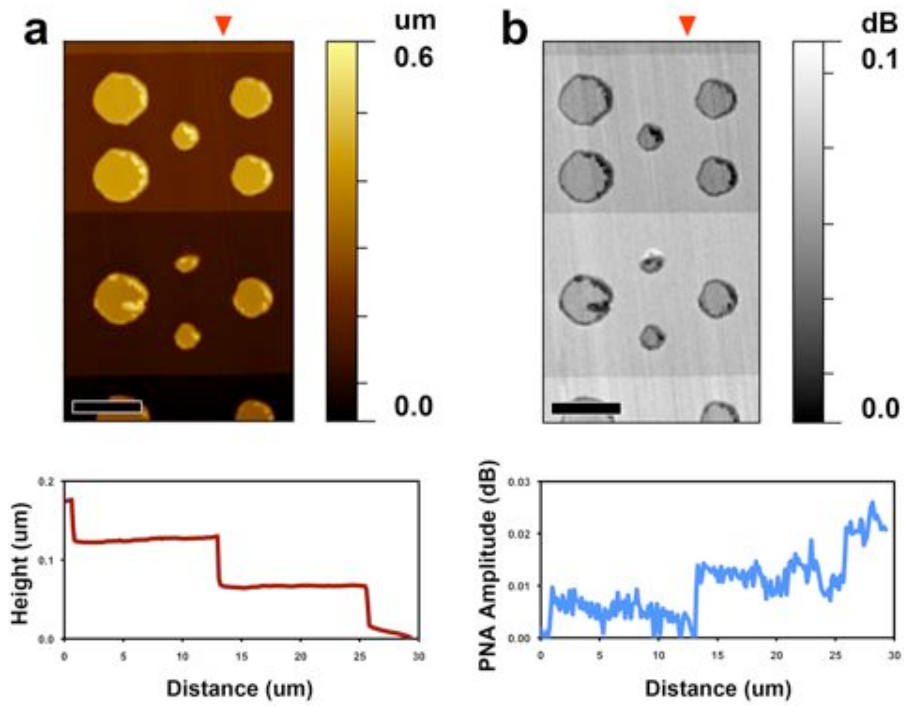

Figure 5. SMM imaging Topographic (a) and capacitive (b) images of a calibration standard collected simultaneously with SMM. Below each image is plotted a line scan from the image, measured from top to bottom at the location of the red arrow. PNA amplitude is the output of the SMM hardware and scales with capacitance. Scale bar is 5 μm.

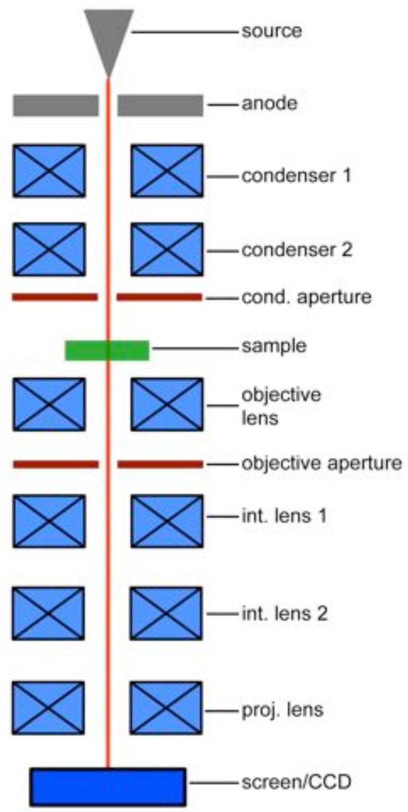

Figure 6. Schematic of a transmission electron microscope Cross-sectional illustration of the components in TEM. See text for descriptions.

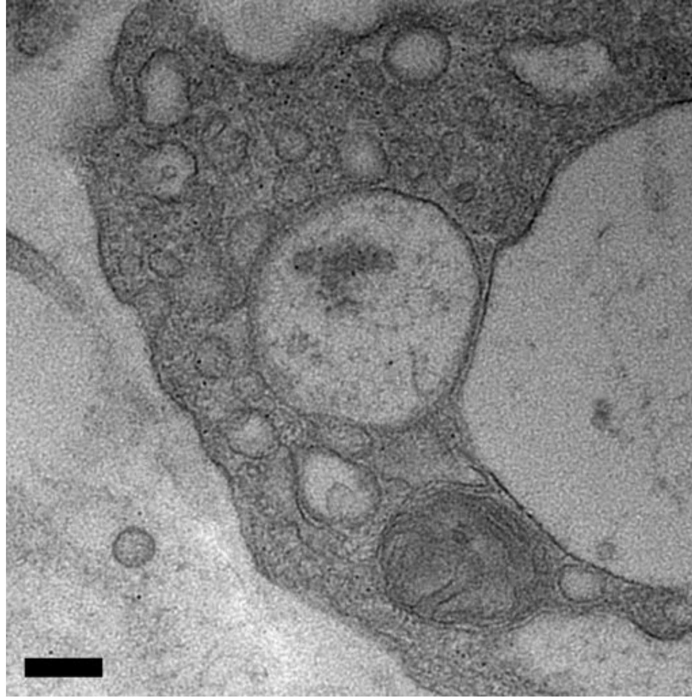

Figure 7. TEM image of biological material Image of a rat kidney cell, sectioned by ultramicrotome and stained with osmium tetroxide. Scale bar is 200 nm.

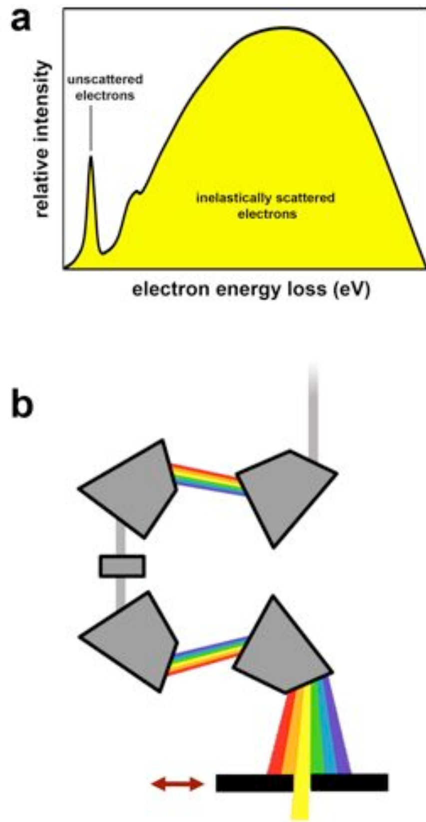

Figure 8. Energy filtering TEM for contrast tuning (a) Plot (not real data) of electron energy loss spectrum, showing unscattered and inelastically scattered populations. (b) "Omega filter" schematic, showing prismatic effect on electron beam in line with the optical axis. The aperture (bottom) can be moved to select for a given energy range (i.e. a given vertical slice through the plot shown in (a))

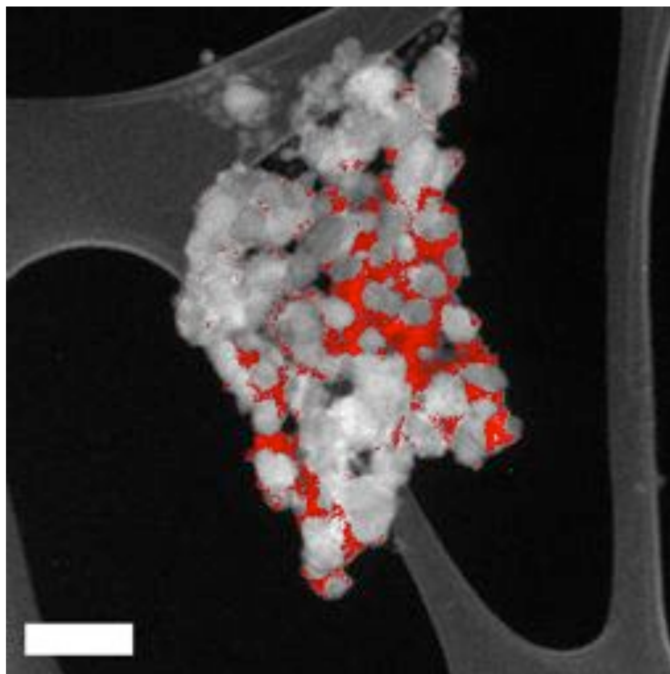

Figure 9. EELS imaging Dark field TEM image of nanoparticles on a lacy carbon grid. Red overlay shows the location of Fe as determined by energy-filtered EELS imaging. Scale bar is 200 nm.

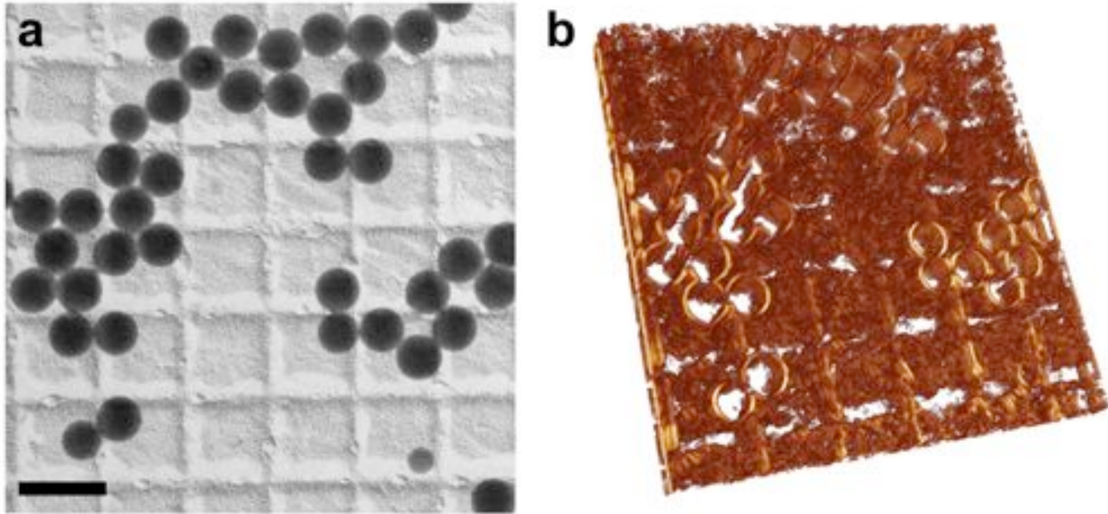

Figure 10. TEM tomography (a) Planar bright field TEM image of 50 nm beads supported by a grid. Scale bar is 100 nm. (b) Tomography of the same sample, computed from multiple images taken at various axial tilt angles relative to the beam.

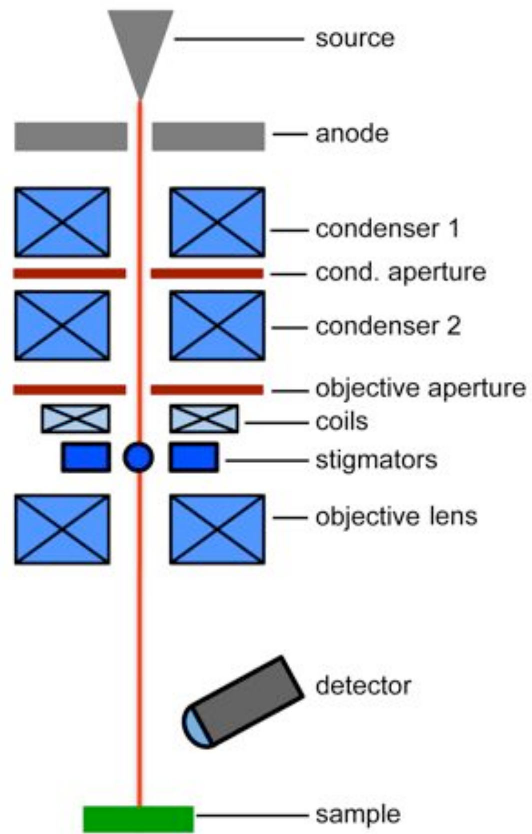

Figure 11. Schematic of a scanning electron microscope Cross-sectional illustration of the components in SEM. See text for descriptions.

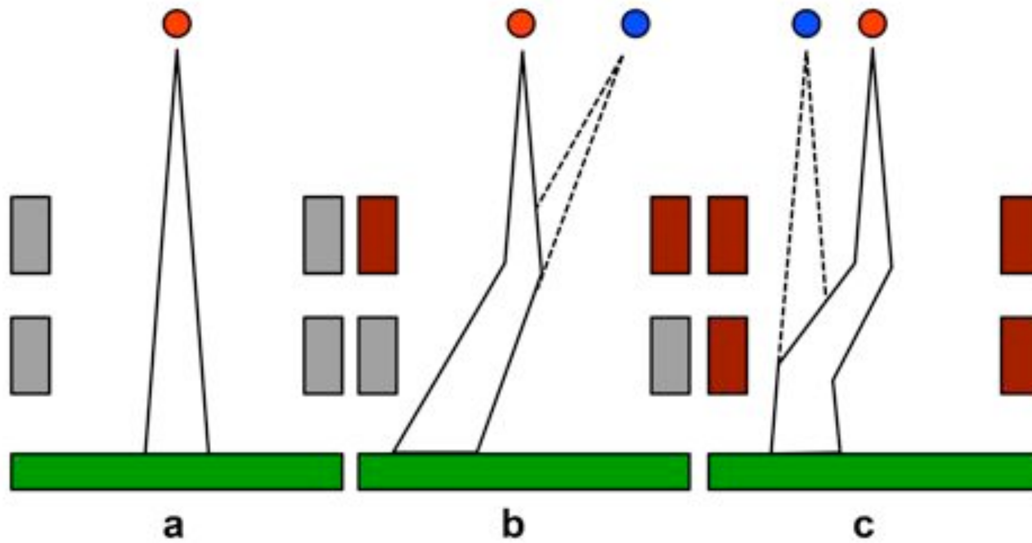

Figure 12. Beam scanning with coils (a) The electron beam path through non-energized deflection coils (red circle represents actual beam source). (b) Using a single set of coils moves the beam to a new lateral position, resulting in a virtual source (blue circle), but also a tilted beam path. Notice the elongated beam at the surface below. (c) Two coil sets in tandem can be used to maintain spot shape while moving the beam to a new location with a beam path parallel to the original.

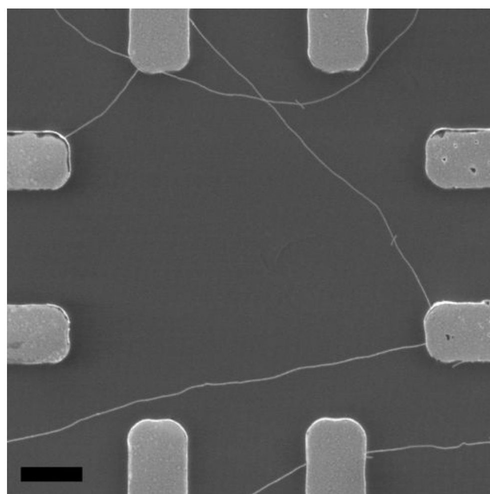

Figure 13. SEM image of nanomaterials SEM image of single-wall carbon nanotubes (bright strings, diameter ~1 nm) pinned under lithographically-defined metal electrodes on a silicon oxide substrate. Scale bar is 5 μm.

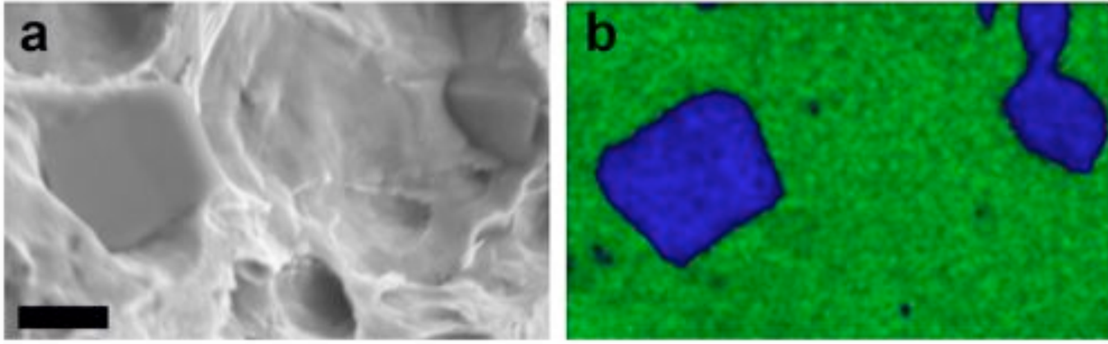

Figure 14. Energy dispersive X-ray mapping (a) SEM image of an alloy material. Scale bar is 2 μm. (b) EDX map of the same field of view, showing the location of Al (green) and Mg (blue).

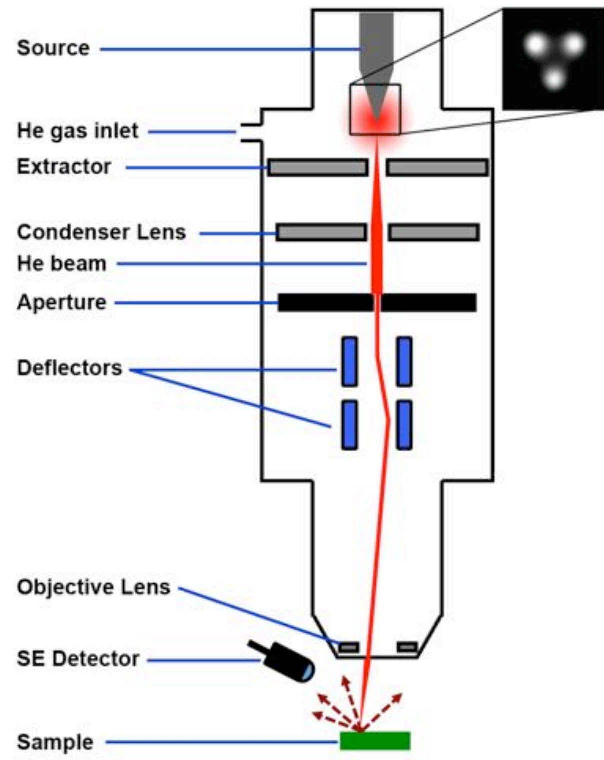

Figure 15. Helium ion microscope A simplified cross-sectional illustration of the components in HIM. Top inset: view of three atoms forming the atomically-small source tip.

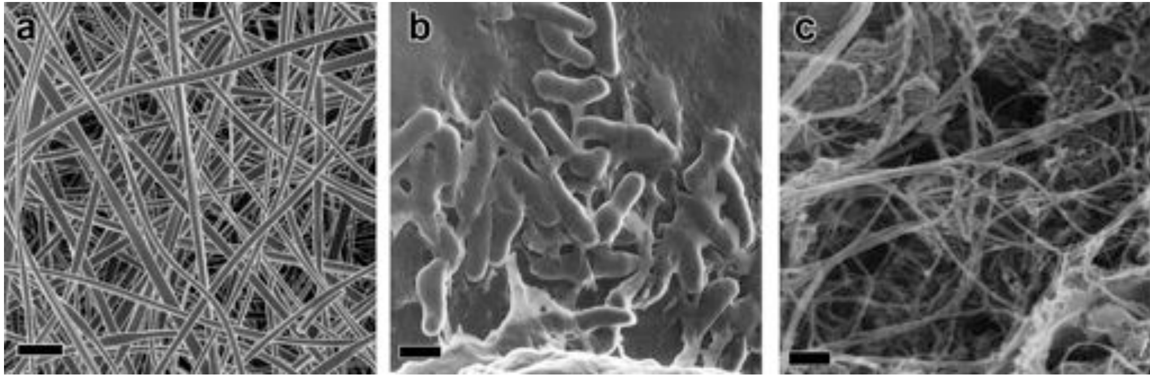

Figure 16. HIM images (a) Electrospun polymeric fibers. Scale bar is 5 μm. (b) Uncoated bacteria. Scale bar is 1 μm. (c) Single-wall carbon nanotube. Scale bar is 100 nm.